

Study on Flow Characteristics of Helium Turboexpander with a Novel Intake Structure

L. Chen^{1†}, B. Meng², Z. Zhang² and Y. Xiao²

¹*College of Environmental and Energy Engineering, Beijing University of Technology, Beijing 100124, China*

²*School of Mechanical Engineering, Beijing Institute of Petrochemical Technology, Beijing 102617, China*

†*Corresponding Author Email: chenlei_bjut@163.com*

(Received May 2, 2021; accepted February 23, 2022)

ABSTRACT

The cylindrical volute intake structure possesses some advantages including convenient processing, convenient installation & uninstallation and high machining efficiency. The helium turboexpander with this novel intake structure in a superconducting cryogenic device is investigated deeply in this study. Based on the established mathematical model and the corresponding numerical computation methods, the whole flow passage internal flow of the helium turboexpander is numerically simulated. And then the distribution characteristics of total pressure, static pressure, static temperature, relative velocity and total enthalpy in the cylindrical volute, nozzle, impeller and diffuser are explored, and loss mechanism of the internal flow is analyzed. The results indicate that the novel cylindrical volute intake structure has obvious pre-rotation effect on the inlet flow field of the nozzle, and this intake structure has little loss. In addition, the expansion effect in downstream components including nozzle and impeller is obvious, and the flow field changes uniformly. The overall efficiency of the turboexpander is up to 84.8%, which indicates that it is reasonable that the novel cylindrical volute is used as the intake structure of turboexpander.

Keywords: Helium turboexpander; Cylindrical volute intake structure; Numerical simulation; Flow characteristics.

NOMENCLATURE

C_{b1}	first empirical constant of S-A model	T	temperature
C_{b2}	second empirical constant of S-A model	t	time
c_p	specific heat capacity	\mathbf{u}	velocity vector
C_{w1}	third empirical constant of S-A model	u_i	velocity component
d	distance to the wall	μ_t	turbulent dynamic viscosity
f_{v1}	coefficient of humidity	x_i	coordinate component
f_w	attenuation function	λ	thermal conductivity
g_i	gravitational acceleration component	μ	viscous dynamic viscosity
p	pressure	$\tilde{\nu}$	turbulent kinematical viscosity
S_T	source term	ρ	density
\tilde{S}	vorticity function	σ	forth empirical constant of S-A model

1. INTRODUCTION

With the rapid development of science, technology and economy, the exploration of science gradually transfers from the conventional field to the extremely harsh environmental field, such as outer space environment, low-temperature environment and so on. In recent years, superconducting technology has been widely used in scientific research and industry fields, such as nuclear fusion experimental device,

high energy particle accelerator, superconducting magnet energy storage system, magnetic fluid, chemical analysis, medicine, magnetic suspension technology, superconducting power transmission and so on. This technology is developed into a certain scale and has great prospect (Ye *et al.* 2010, Hu *et al.* 2014). The low-temperature environment is an essential condition for the achievement of superconducting technology. And this environment is generally achieved by depending on cryogenic

system. The key component of the cryogenic system is the helium turboexpander, so it is of important practical significance to study the performance of the helium turboexpander for the improvement of efficiency and the optimization of working parameters of the whole cryogenic system.

The working principle of turboexpander is similar to that of turbocharger, and the research methods involved in them can be used to refer from each other. Therefore, these studies can provide important reference for the performance research of turboexpander in this paper. In the research fields of turboexpander and turbocharger, the numerical simulation and experimental research on different working medium and different structural parameters have been conducted by many scholars, and some research results are obtained. [Watanabe *et al.* \(1971\)](#) constructed an experimental radial-inflow turbine with a pressure ratio of 2:1. The performance test of the turbine was carried out by adopting compressed air, and the influence of the size parameters of the impeller was investigated. Based on the numerical simulation, [Singhal and Spalding \(1981\)](#) compared the predicted results with the experimental results. The results indicated that the $k-\epsilon$ model of turbulence can predict the two-dimensional turbulent boundary layer with non-uniform streamwise pressure gradient and infinite sweeping condition. [Whitfield \(1990\)](#) introduced the dimensionless design method of radial-inflow turbine rotor, and pointed out that all dimensionless performance parameters could be determined through the dimensionless design calculation of the turbine rotor. For a specific design condition, [Ino *et al.* \(1992\)](#) developed a radial-inflow turbine with high expansion ratio, and provided the specific design results. According to the performance characteristics of radial-inflow turbine applied in small gas turbine, [Rodgers \(2003\)](#) discussed the importance of turbine velocity ratio selection on rotor tip diameter and cycle performance, and studied the influence of rotor reaction on flow versus pressure characteristics of radial-inflow turbine. To overcome the defects of traditional design method of cylindrical parabolic impeller, [Feng *et al.* \(2005\)](#) proposed a design method in which the positive axial displacement and skew technique were combined, and redesigned a novel impeller with good aerodynamic performance and strength reliability. In addition, the turbulent flow characteristics inside the impeller were simulated and analyzed in detail. [Deschildre *et al.* \(2008\)](#) developed a dynamic model of helium refrigerator, which was simulated by using the Aspen Hysys software. Based on the results of numerical simulation, the detailed analysis was carried out, and some advantages of the developed model were pointed out. [Ghosh *et al.* \(2010\)](#) developed a small high-speed cryogenic turboexpander in which the pneumatic thrust bearing was adopted, and studied the influence of bearing vibration on the performance and stability of turboexpander. [Cheng *et al.* \(2010\)](#) used different modules of ANSYS software to model blades of turboexpander impeller and brake compressor wheel, and numerical simulation on the designed model was implemented and the

distribution of flow field was obtained. In view of the high-speed expanded turbine with nitrogen as the flow medium, [Dimri *et al.* \(2013\)](#) adopted CFD software to simulate it, and obtained the change trend of velocity, pressure, temperature, entropy and Mach number along the streamline and spanwise, and analyzed the flow characteristics of cryogenic turboexpander. [Shah *et al.* \(2014\)](#) described the dimensionless design procedure of a vaneless turbine volute in compressible flow regime, and investigated the variation of design parameters including area ratio and radius ratio with azimuth angle, and comparatively researched three different volute cross sections. [Sauret and Gu \(2014\)](#) provided the complete design procedure of R143a radial-inflow turbine, and compared the results of meanline analysis with the results of three-dimensional viscous simulation. In addition, the parametric research was carried out, the necessity of a coupled optimization of thermodynamic cycle and one-dimensional turbine design was pointed out. To qualitatively and quantitatively explain phenomena of flow distortion and rotor resonance in the radial-inflow turbine with vaneless volute, [Huang *et al.* \(2017\)](#) studied the forced response mechanism of the radial-inflow turbine based on a fluid structure interaction method, and analyzed the effect of volute tongue on the low distortion and response force of the turbine rotor. To verify the effectiveness of the blade design of helium cryogenic turboexpander, [Meng *et al.* \(2017\)](#) utilized two kinds of software including NUMECA and CFX to carry out numerical simulation of the designed turboexpander under the design condition, and detailedly analyzed the flow characteristics of helium cryogenic turboexpander on the basis of numerical results. For the turboexpander with cryogenic helium as working medium, [Li *et al.* \(2018\)](#) implemented whole flow passage numerical simulation on three different aerodynamic guide cascades by using CFX software, and compared the performance of three different aerodynamic cascades under the design conditions. Moreover, the change law of guide cascade performance with the number of blades was obtained. By using Matlab, [Niu *et al.* \(2018\)](#) conducted mathematical prediction research on the performance of cryogenic turboexpander under varied operating conditions, and analyzed influences of pressure ratio, inlet temperature and speed change on turbine performance. In addition, the off-design performance prediction results and experimental test results of cryogenic turboexpander were compared and analyzed. By using two different loss indicators, i.e. total pressure loss and entropy generation rate, [Tanganelli *et al.* \(2019\)](#) analyzed the sources of thermodynamic irreversibilities in different volutes of compressor, and evaluated the influence of loss mechanism under the design and off-design conditions.

In previous studies, the snail-type volute is generally adopted in the intake structure of turboexpander. The actual cutting operation of snail-type volute is carried out by using the cutting tools of different sizes and diameters, which is a complex and tedious work.

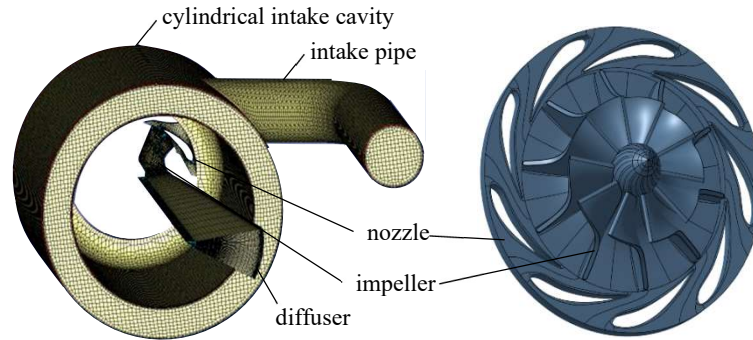


Fig. 1 Structural schematic of helium turboexpander.

Table 1 Dimensional parameters of intake structure

Intake pipe	Diameter (mm)	Length of inlet section (mm)	Area of middle crooked section (mm ²)
	22.4	92.43	2763.39
	Perimeter of middle crooked section (mm)	Area of outlet section (mm ²)	Perimeter of outlet section (mm)
	140.74	2570.61	172.5
Cylindrical intake cavity	Inner cylindrical diameter (mm)	Cylindrical thickness (mm)	External height (mm)
	67	11.5	101.3
	Outlet inner circle diameter (mm)	Outlet height (mm)	Bottom chamfer radius (mm)
	50	2.67	14

Many important holes and machining surfaces are located in three-dimensional space, which brings great difficulties to machining and measurement (Wang 2013). Thus, it is difficult to ensure high machining accuracy of snail-type volute. To overcome the defects in the machining of snail-type volute, a novel type of intake structure which is easy to machine, is designed in this study. In the machining process of the novel cylindrical volute intake structure, only the diameter of inner cylinder, diameter of outer cylinder, height of cylinder and radius of fillet at the bottom are required to determine the dimension of the cylindrical part. A lot of cutting tools with different diameters which are generally applied to cut the circular arc wall of snail-type volute, are barely needed in the machining process of novel cylindrical volute intake structure. To some extent, the error caused by different cutting experience is avoided efficiently. In addition, the design of fixture for machining machine worktable is simpler than the former, and the overall installation and disassembly are also more convenient. Not only can the precision of the processing be ensured, but also the processing speed and production efficiency can be improved. However, the internal flow characteristics of this novel intake structure is unclear. Therefore, the study on the internal flow characteristics of whole flow passage of helium turboexpander with the cylindrical volute structure is conducted in this paper. This study makes us have a deeper understanding for the internal flow of helium turboexpander with this novel intake structure. In

addition, it could provide a significant reference for the future optimization research on the helium turboexpander with this novel intake structure.

2. MATHEMATICAL MODEL

The structural schematic of helium turboexpander is shown in Fig. 1, and the structural parameters of intake structure are shown in Table 1. When the helium turboexpander works, the working medium first streams into the cylindrical intake cavity through the intake pipe in the intake structure. Then, the working medium streams into the nozzle between the two stationary blades at a certain velocity, and the velocity of working medium at outlet position of nozzle increases, and the temperature and pressure decrease. Then the working medium streams into the high-speed rotating impeller at a certain relative velocity, expands further in the impeller and outputs the shaft work. In this process, the pressure decreases, the temperature and velocity of working medium also decrease. At the outlet of impeller, the working medium streams out at a certain velocity and enters the diffuser. A part of the kinetic energy of working medium is converted into the pressure energy by a diffuser, and the temperature and pressure of working medium at the outlet of diffuser increase and the velocity decreases.

To quantitatively describe the flow and heat transfer process of helium in a turboexpander, it is necessary to establish a three-dimensional

mathematical model, including governing equations, boundary conditions and initial conditions in general. This flow and heat transfer process meet three conservation laws. Therefore, three conservation equations are used to describe this process in this study, including continuity equation, momentum equation and energy equation, as shown in Eq. (1) - Eq. (3) (Tao 2001, Zhang *et al.* 2019, Deng *et al.* 2019). The flow of helium in a turboexpander is generally turbulent flow. To describe this kind of flow, the Spalart-Allmaras turbulence model is adopted in this paper, and its expression is shown in Eq. (4) (Spalart and Allmaras 1994). The main reason for using this turbulence model is that the viscosity field of turbulence vortex obtained by using this model is always continuous. Compared with k-ε model, this model exhibits better stability and robustness, and generally possesses higher numerical simulation efficiency (Yan 2011). The Spalart-Allmaras turbulence model is related to the momentum equation by Eq. (5). Therefore, for the flow and heat transfer numerical simulation of turboexpander, the governing equations include Eq. (1) - Eq. (5).

$$\frac{\partial \rho}{\partial t} + \frac{\partial (\rho u_i)}{\partial x_i} = 0 \quad (1)$$

$$\frac{\partial (\rho \mathbf{u})}{\partial t} + \frac{\partial (\rho u_i \mathbf{u})}{\partial x_i} - \frac{\partial}{\partial x_i} \left[(\mu + \mu_t) \frac{\partial \mathbf{u}}{\partial x_i} \right] = - \frac{\partial p}{\partial x_i} + \rho \mathbf{g}_i \quad (2)$$

$$\frac{\partial (\rho c_p T)}{\partial t} + \frac{\partial (\rho c_p u_i T)}{\partial x_i} = \frac{\partial}{\partial x_i} \left(\lambda \frac{\partial T}{\partial x_i} \right) + S_T \quad (3)$$

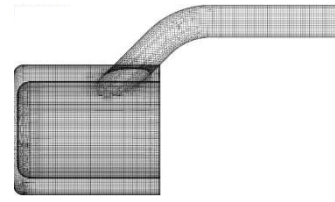
$$\frac{\partial (\rho \tilde{v})}{\partial t} + \frac{\partial (\rho u_i \tilde{v})}{\partial x_i} = C_{b1} \rho \tilde{S} \tilde{v} - C_{w1} \rho f_w \left(\frac{\tilde{v}}{d} \right)^2 + \frac{1}{\sigma} \left\{ \frac{\partial}{\partial x_i} \left[(\mu + \rho \tilde{v}) \frac{\partial \tilde{v}}{\partial x_i} \right] + C_{b2} \rho \left(\frac{\partial \tilde{v}}{\partial x_i} \right)^2 \right\} \quad (4)$$

$$\mu_t = \rho \tilde{v} f_{v1} \quad (5)$$

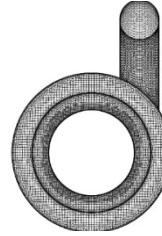
Besides the above governing equations, the boundary conditions should be included in the mathematical model. For the numerical simulation in this paper, the temperature and pressure boundary conditions are adopted at the inlet of turboexpander. The total temperature and total pressure at the inlet are set as 73.16K and 1.75MPa, respectively. The pressure boundary condition is adopted at the outlet of turboexpander, and the static pressure at the outlet is set as 0.85MPa. In addition, the adiabatic and no-slip boundary conditions are adopted for the wall, and the periodic boundary condition is adopted between the nozzle and the impeller. The initial condition in this study is a static field.

3. NUMERICAL SIMULATION METHOD

Based on structured grid and unstructured grid generation technologies, the node control method is adopted to divide mesh in this paper, and the grid density is controlled by setting the position of main nodes on the grid surface, so as to achieve the



(a) Side view



(b) Front view

Fig. 2. Divided grid of intake structure.

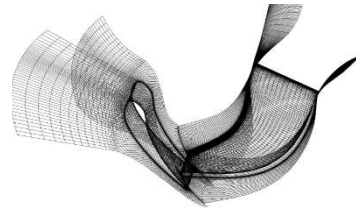


Fig. 3. Divided grid of nozzle and impeller.



Fig. 4. Divided grid of meridian plane (the lower right corner roughly shows divided grid of diffuser).

purpose of improving the grid quality (Ke *et al.* 2018). According to this grid division method, the grids used to divide the intake structure, nozzle, impeller, diffuser and meridian plane of turboexpander are obtained, as shown in Fig. 2, Fig. 3 and Fig. 4. There are 535876 grids in the intake structure, and 861354 grids in nozzle, impeller and diffuser. In total, there are 1.4 million grids in the whole machine. This grid system is utilized for the numerical simulation, and the numerical results could meet the requirement of grid independence.

Based on the above divided grids, the governing equations are discretized by the finite volume method, in which the time term is discretized by forward difference scheme, and the convection term is discretized by the second-order upwind scheme, and the diffusion term is discretized by the central difference scheme.

After the discrete equations are obtained, the coupling solution of the discrete equations corresponding to the different governing equations is realized by using the SIMPLE algorithm. The preconditioned conjugate gradient method is adopted as the solver of equations, and the multigrid technique is adopted to accelerate convergence of solution.

4. RESULTS AND ANALYSIS

To further understand the internal flow characteristics in the different components of helium turboexpander with novel intake structure, based on the above numerical simulation methods, the parameter distribution characteristics of helium turboexpander are investigated, and the internal flow loss mechanism is analyzed.

4.1 Flow Analysis for the Cylindrical Volute

In this section, the cylindrical volute and its cross section are selected to research the parameter distribution of novel volute. The distributions of static pressure, static temperature, total enthalpy and relative velocity in the cylindrical volute composed of intake pipe and cylindrical intake cavity are shown in Fig. 5(a)-(d). It can be seen from the Fig. 5(a) and Fig. 5(d) that the static pressure distribution in the intake pipe is relatively uniform. Only at the crooked position of the intake pipe, the pressure at the outer side is slightly higher than the pressure at the inner side. The reason of this slightly uneven pressure is that the impact force of entrance helium on the outer wall of the intake pipe is larger than that on the inner wall. In general, the larger the impact on the outer wall, the higher the pressure and the lower the speed. The pressure near the outlet position of intake pipe is close to the inlet pressure of helium turboexpander and higher than the pressure on whole surface of cylindrical intake cavity. This phenomenon is induced by relatively sufficient flow and consistent pressure of the helium in the large-diameter intake pipe. When the helium enters the narrow cylinder gap, the flow is seriously blocked. Therefore, the surface of the cylindrical intake cavity facing the outlet of the intake pipe, bears large pressure and shows low velocity. As the helium continues to flow into the large cavity of the cylindrical intake cavity, the flow obstruction phenomenon is obviously weakened, the velocity increases and the pressure decreases.

The intake pipe is designed according to the eccentric structure principle. The helium entering the cylindrical intake cavity in the direction of along eccentric structure has certain advantages over that in other directions. Therefore, the velocity in the direction of along eccentric structure is higher than that in other directions. In addition, the total enthalpy is lower and the loss is smaller. On the other hand, we can also see different color distributions with the triangular shape from Fig. 5 (a) to Fig. 5 (d), which seems that the flow parameters in this novel cylindrical intake cavity are uneven and there seems to be a large flow loss. However, from a quantitative point of view, the pressure in the cylindrical intake cavity fluctuates within 1kPa and the temperature fluctuates within 0.1K, and thus the variation range is relatively small, and there is no large flow loss. According to the analysis of the flow parameters of the cylinder volute intake structure, it can be known that the novel cylinder volute structure is not the main cooling component, but mainly plays the role of diversion.

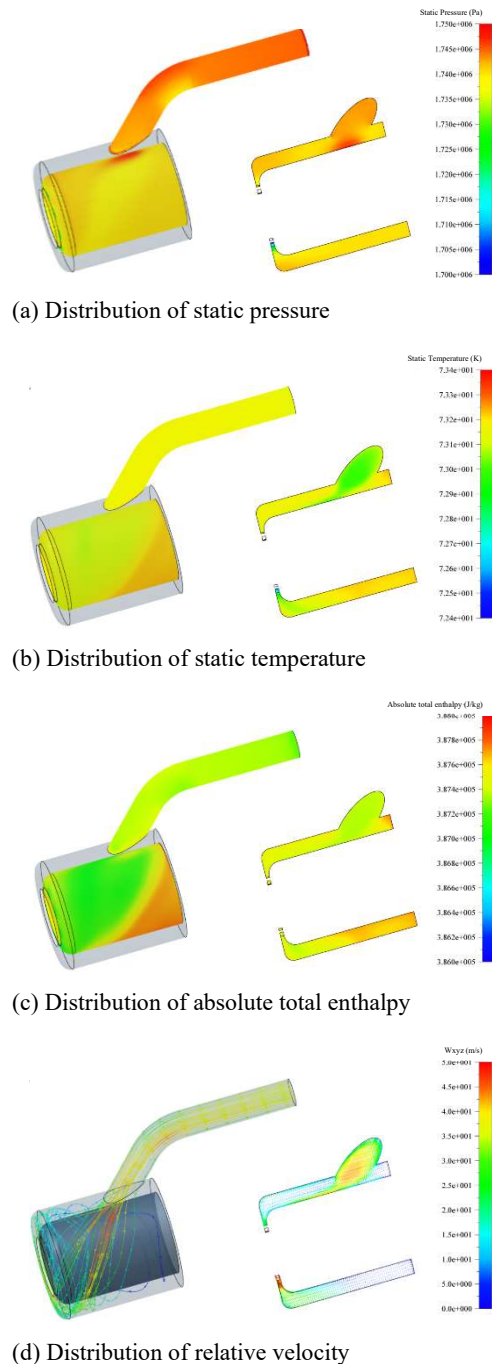


Fig. 5. Distribution of static pressure, static temperature, total enthalpy and relative velocity of cylindrical volute.

4.2 Flow Analysis for the Nozzle and Impeller S1 Surface

The distributions of total enthalpy, static pressure, static temperature and relative velocity on 10%, 50% and 90% blade height sections of S1 surface are shown in Fig. 6.

The distribution of static pressure is shown in Fig. 6(a), it can be found that the stream stagnation point in the nozzle falls on the pressure side, and the gas stream continuously accelerates along the flow

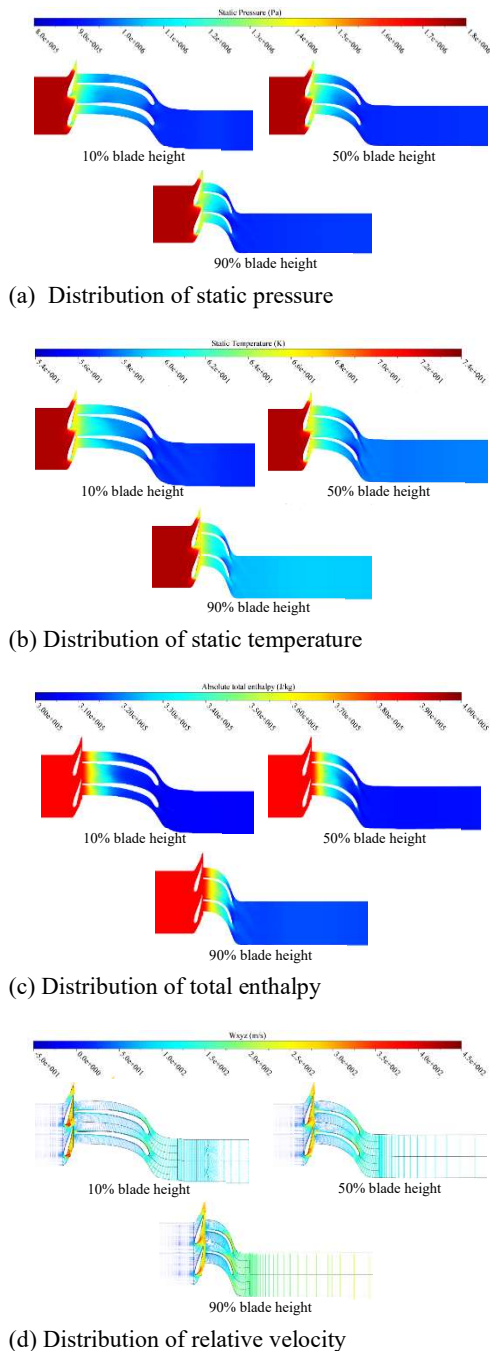
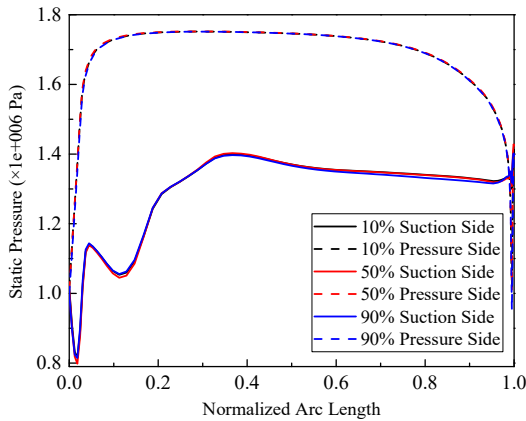


Fig. 6. Distribution of static pressure, static temperature, total enthalpy and relative velocity on different blade height sections of S1 surface.

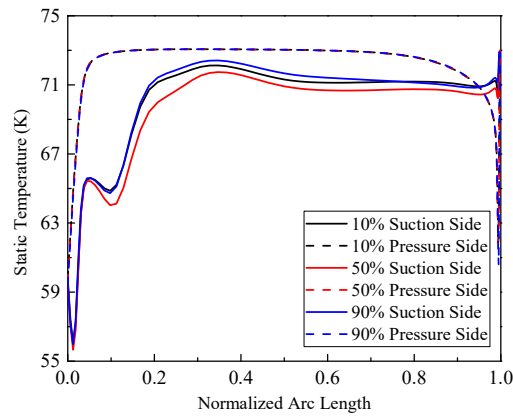
direction of working medium from the stagnation point position on the pressure side. The pressure gradient along the trailing edge of pressure side changes evidently, and the expansion and cooling process is obvious. The gas stream from the stagnation point to the suction side needs to bypass the front of whole blade before reaching the suction side, where the stream is prone to over expansion. The velocity distribution demonstrates that the stream does not separate. After bypassing the front of nozzle blades, the stream continues to flow

downstream along the suction side and accelerates in the flow passage. It can be known from the above that the expansion and cooling process of working medium in the nozzle passage mainly occurs at the outlet position of flow passage. In the impeller passage, as the working medium flows, the working medium pressure decreases gradually, and the force of gas on the impeller structure also decreases gradually. The static pressure value of pressure side is higher than that of suction side at the corresponding position. Due to the pressure difference between the two sides, the impeller is driven and the external work is output. In addition, with the increase of blade height, the position of relatively high pressure gradient in the flow passage gradually shifts to the top of impeller blades.

There is a wake flow phenomenon at the tip of trailing edge, which is related to the clearance flow at the top of impeller blades. It can be seen from Fig. 6(b) that the changing trend of static temperature on different blade height sections on the same side of nozzle passage is similar to the changing trend of static pressure. In addition, the difference of static temperature between pressure side and suction side is not obvious. According to the Fig. 6(b), the distribution of static temperature of impeller blades is generally uniform, but the distribution uniformity is slightly worse than that of static pressure. In the 20% entrance chord length from the front edge, the temperature of root and top of blade on both sides is higher, and the temperature of corresponding point of blade root and top in the suction side is higher than that in the pressure side. The above is caused by the impact and scraping effect of high-speed stream on the blade tip. Along the direction of flow, the temperature distribution in the impeller passage tends to be uniform and the temperature decreases gradually. It can be seen from Fig. 6(c) that the total enthalpy distribution of working medium on the whole S1 surface is relatively uniform, and the total enthalpy in the nozzle on different blade height sections barely changes, which is consistent with the enthalpy value at the inlet. After the working medium streams into the impeller, a part of internal energy is converted into mechanical energy, and the work is output through the rotating shaft. Due to this reason, the total enthalpy of working medium in the impeller passage decreases with the flow continuously. The relative velocity vector distribution is shown in Fig. 6(d), which indicates that the relative velocity direction in the nozzle is generally along the blade profile. There is an obvious low-pressure point at the 3% position from the front of suction side, in which the relative velocity deviates evidently. This phenomenon is related to the position of stagnation point on the pressure side and the large curvature change of nozzle blades front. In general, the stream distribution is relatively ideal. In addition, in the impeller passage, the inlet of impeller blade meets the condition of vertical intake, and the relative velocity vector distribution along the chord length almost fits the blade profile. The velocity at the trailing edge of the top section of impeller blades increases obviously, which induces the loss of wake flow in a certain.



(a) Static pressure



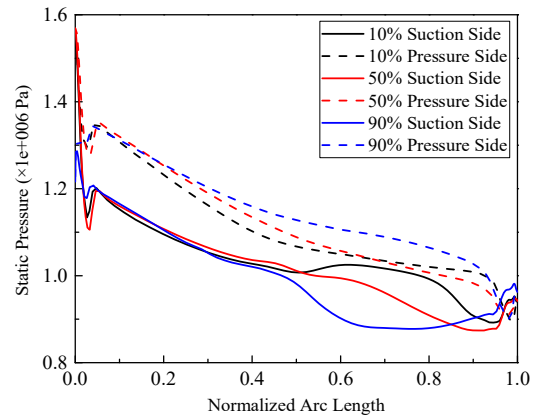
(b) Static temperature

Fig. 7. Distribution curves of static pressure and temperature at the nozzle blade surface.

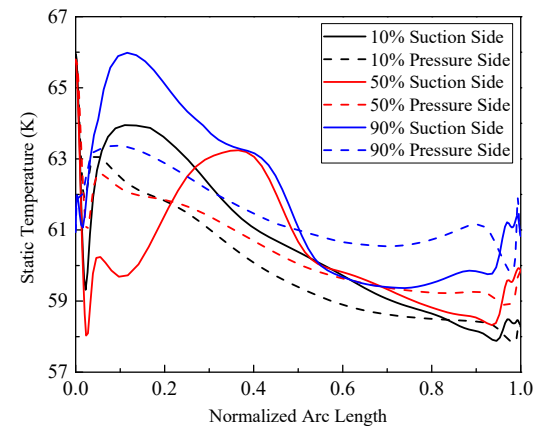
4.3 Flow Analysis for the Nozzle and Impeller Blade Surface

The distribution curves of static pressure and static temperature of nozzle and impeller blade surface of helium turboexpander at three different blade height sections are shown in Fig. 7 and Fig. 8, respectively. The static pressure and temperature distribution are given on the three-dimensional blade surface of nozzle and impeller, as shown in Fig. 9, in which the changing process of parameters from different span and blade height shroud can be directly seen.

From the Fig. 7(a), it can be seen that the static pressure change of stream on different height positions on the same side is similar, and the static pressure on the suction side is lower than that on the pressure side. The static pressure fluctuation at the front of nozzle blade is relatively obvious under the influence of flow angle. Besides, due to the influence of the throat position, the fluctuation of static pressure at the suction side is more violent than that at the pressure side. At the position of 60% and more than chord length, the static pressure exhibits continuous decreasing trend. The velocity at the outlet of pressure side increases evidently, which indicates that the pressure-decrease and velocity-increase process is achieved well near the outlet of



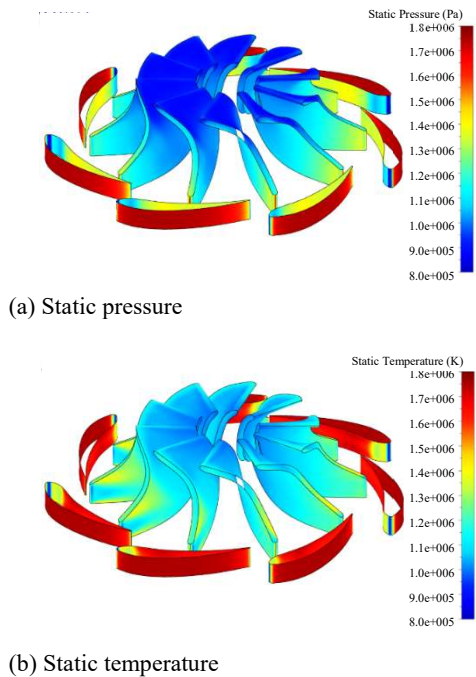
(a) Static pressure



(b) Static temperature

Fig. 8. Distribution curves of static pressure and temperature at the impeller blade surface.

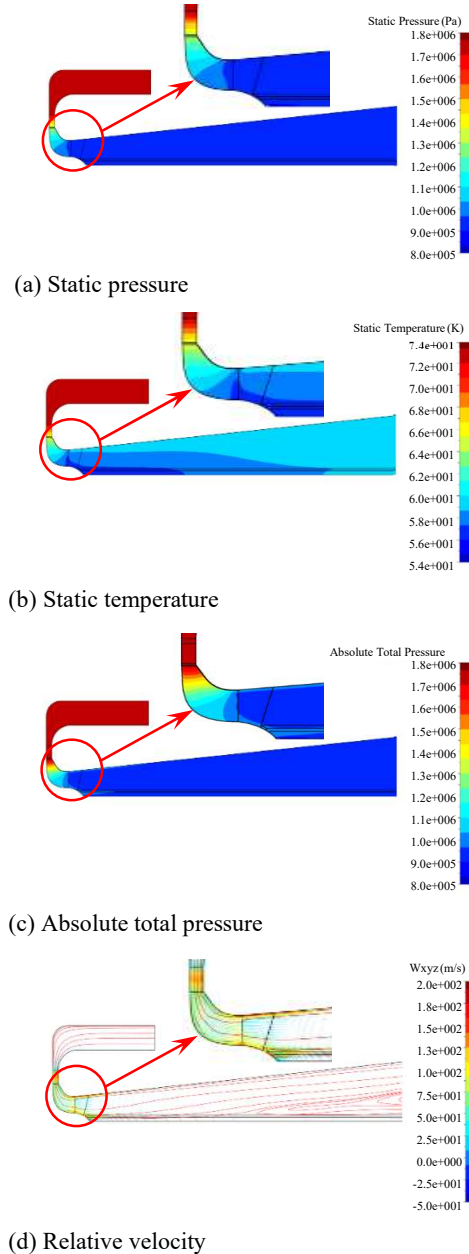
flow passage. The phenomenon corresponds to the varies of static pressure and relative velocity on the S1 surface mentioned in the section 4.2. In the Fig. 7(b), the changing trend of temperature in the nozzle is similar to the pressure. Except for the rise and fall of temperature at the front of suction side, the overall temperature difference on both sides of blades has little change. It can be seen from the Fig. 8(a) that the static pressure on both sides of blades overall shows a decreasing trend, and the pressure distribution on the same side of radial flow section of impeller blades on different blade height direction is almost consistent. It could be assumed that the force on the blade along the height direction is relatively uniform. On the axial flow section, the pressure fluctuation at the trailing edge of suction side is obvious, and the pressure at the blade top of trailing edge position decreases evidently. In the Fig. 8(b), affected by the impact and scraping effect of high-speed stream, the temperature change of blade root and tip is relatively obvious, and the temperature on the intermediate section at the inlet position of impeller blades is relatively low. On the whole, the parameter distribution of impeller blades accords with the flow feature of general turboexpander.



(a) Static pressure
(b) Static temperature
Fig. 9. Distributions of static pressure and temperature at the nozzle and impeller blade surface.

4.4 Flow Analysis for the Meridional Plane of Helium Turboexpander

As the flow field in the intake structure is asymmetric, only the flow field of nozzle, impeller and diffuser is treated by the density weighted circumferential averaging method. The distribution of total pressure, static pressure, static temperature and relative velocity after circumferential average is shown in Fig. 10(a)-(d). It can be found that the working medium expands and cools down in the nozzle, and its velocity increases. Moreover, the total pressure almost remains unchanged. Along the direction of flow, the static pressure distribution from the root of blade to the top in the nozzle is uniform. The changing trends of static temperature and static pressure are almost the same in the nozzle. The gas stream from the nozzle expands continuously in the impeller. Owing to the mechanical energy exchange between the gas in the impeller and the outside environment, the pressure and temperature of working medium decrease continuously, and the relative velocity of gas stream also decreases. In the impeller, the total pressure decreases gradually and exhibits the U-shape changing trend. The load is relatively large at the root position of blade outlet in the impeller flow passage. In the inlet region, the temperature of impeller near the hub and shroud sides is relatively high, and the temperature at the middle position is relatively low. Along the direction of flow, the low temperature area gradually shifts to the root of impeller. The gas stream from the impeller outlet decelerates gradually in the diffuser and its pressure enlarges. There is a temperature gradient from the outer edge of diffuser to the axis, and there is a vortex area in the surrounding of axis at the diffuser outlet, which is caused by the reverse pressure gradient, but the



(a) Static pressure
(b) Static temperature
(c) Absolute total pressure
(d) Relative velocity
Fig. 10. Distributions of static pressure, static temperature, total pressure and relative velocity of meridional plane.

vortex area has little influence on the flow of gas stream inside the diffuser.

5. CONCLUSIONS

For the helium turboexpander with a novel cylindrical volute intake structure, its flow characteristics are researched on the basis of numerical simulation. The distributions of total pressure, static pressure, static temperature, relative velocity and total enthalpy in the turboexpander are investigated, and the internal flow loss is analyzed in detail. The main conclusions are drawn as follows:

- (1) The novel cylindrical volute has advantages of machining convenience and high machining efficiency. The flow in the intake pipe of cylindrical

volute is relatively uniform. Under the influence of eccentric structure, the flow parameters of helium in cylindrical intake cavity vary in a small range, but the parameter distribution is uniform as a whole.

(2) In the nozzle, the changing trend of static pressure in the identical side of the nozzle is almost same on the different blade height sections. In addition, the relative velocity of helium in the nozzle is mainly distributed along the blade contour, and there is no obvious vortex and reflux. In the impeller, the temperature distribution in the flow passage is relatively uniform, and the temperature is relatively high only in the root and tip of the suction side of blade inlet. On the other hand, the relative velocity of helium in the flow passage is almost distributed along the blade contour, which conforms to the flow characteristics of helium in the impeller. In the diffuser, along the flow direction, the pressure increases gradually, and the speed decreases gradually. The temperature gradient from the center of diffuser to the outer wall is almost uniform.

(3) In general, the intake pipe designed according to the eccentric structure principle has obvious pre-rotation effect on the flow at the inlet zone of nozzle, and the overall loss in the novel cylindrical volute is small. The expansion effect of helium in the nozzle and impeller is obvious, and the parameter distributions of the flow passage change evenly, and the loss is relatively small. The diffuser has obvious diffusion effect, and the parameter distributions of the flow passage change evenly and the loss is unobvious. The above results indicate that it is reasonable to use the novel cylindrical volute as the intake structure of the turboexpander.

REFERENCES

- Cheng, A., B. Fu and Q. Zhang (2010). Turbo-shape design method of helium turbo-expander. *Cryogenics* 5, 33-36.
- Deng, Y., L. Zhang, H. Hou, B. Yu and D. Sun (2019). Modeling and simulation of the gas-liquid separation process in an axial flow cyclone based on the Eulerian-Lagrangian approach and surface film model. *Powder Technology* 353, 473-488.
- Deschildre, C., A. Barraud, P. Bonnay, P. Briend, A. Girard, J. M. Poncet, P. Roussel and S. E. Sequeira (2008). Dynamic simulation of an helium refrigerator. *AIP Conference Proceedings* 985(1), 475-482.
- Dimri, H. (2013). Computational fluid flow analysis of cryogenic turboexpander. Master Thesis, *National Institute of Technology*, Odisha, INDIA.
- Feng, Z., Q. Deng and J. Li (2005). Aerothermodynamic design and numerical simulation of radial inflow turbine impeller for a 100kW microturbine. *Proceedings of ASME Turbo Expo 2005: Power for Land, Sea, and Air*, Reno-Tahoe, USA.
- Ghosh, S. K., R. K. Sahoo and S. K. Sarangi (2010). Experimental performance study of cryogenic turboexpander by using aerodynamic thrust bearing. *Applied Thermal Engineering* 30(11-12), 1304-1311.
- Hu, J., Z. Zhou, M. Zhuang, B. Fu, L. Yang (2014). Analysis of characteristics and control methods of rotational speed for helium turbine expander. *Cryogenics* 5, 45-51.
- Huang, Z., C. Ma and H. Zhang (2017). Investigation of flow distortion generated forced response of a radial turbine with vaneless volute. *International Journal of Turbo & Jet-Engines* 37(2), 141-151.
- Ino, N., A. Machida, K. Tsugawa, Y. Arai, M. Matsuki, H. Hashimoto and A. Yasuda (1992). Development of high expansion ratio helium turbo expander. *Advances in Cryogenic Engineering* 37, 835-844.
- Ke, C., L. Xiong, N. Peng, K. Li and L. Liu (2018). Thermodynamic parameters calculation and numerical simulation correction for cryogenic turbine expander. *Cryogenics & Superconductivity* 46(11), 24-29.
- Li, X., J. Li and Q. Li (2018). Numerical simulation of flow in the nozzle of cryogenic helium turbo-expander. *Cryogenics & Superconductivity* 46(4), 1-5.
- Meng, Y., L. Xiong, L. Liu and N. Peng (2017). Design and flow performance study of a helium cryogenic turbo-expander. *Cryogenics* 4, 46-54.
- Niu, L., Y. Meng, X. Li, Q. Zeng, F. Lou and Y. Hou (2018). Off-design performance analysis of cryogenic turbo-expander based on mathematic prediction and experiment research. *Applied Thermal Engineering* 138, 873-887.
- Rodgers, C. (2003). The characteristics of radial turbines for small gas turbines. *Proceedings of ASME Turbo Expo 2003: Power for Land, Sea, and Air*, Atlanta, USA.
- Sauret, E. and Y. Gu (2014). Three-dimensional off-design numerical analysis of an organic Rankine cycle radial-inflow turbine. *Applied Energy* 135, 202-211.
- Shah, S. P., S. A. Channiwalla, D. B. Kulshreshtha and G. Chaudhari (2014). Design and numerical simulation of radial inflow turbine volute. *International Journal of Turbo & Jet-Engines* 31(4), 287-301.
- Singhal, A. K. and D. B. Spalding (1981). Predictions of two-dimensional boundary layers with the aid of the $k-\epsilon$ model of turbulence. *Computer Methods in Applied Mechanics and Engineering* 25(3), 365-383.
- Spalart, P. and S. Allmaras (1994). A one-equation turbulence model for aerodynamic flows. *Recherche Aeronautique* 1(1), 5-21.
- Tanganelli, A., F. Balduzzi, A. Bianchini, G. Ferrara, F. Cencherle, M. D. Luca and L. Marmorini (2019). An Investigation on the Loss Generation

- mechanisms inside different centrifugal compressor volutes for turbochargers. *Journal of Engineering for Gas Turbines and Power* 141(2), 021004.
- Tao, W. (2001). Numerical heat transfer (second edition). *Xi'an Jiaotong University Press*, Xi'an, China.
- Wang, J. (2013). High-efficiency numerical control machining technology for the model volute. *Metal Working (Cold Working)* 14, 14-16.
- Watanabe, I., I. Ariga and T. Mashimo (1971). Effect of dimensional parameters of impellers on performance characteristics of a radial-inflow turbine. *Journal of Engineering for Power* 93(1), 81-102.
- Whitfield, A. (1990). The preliminary design of radial inflow turbines. *Journal of Turbomachinery* 112(1), 50-57.
- Yan, C., J. Yu, J. Xu, J. Fan and D. Gao (2011). On the achievements and prospects for the methods of computational fluid dynamics. *Advances in Mechanics* 41(5), 562-589.
- Ye, B., B. Ma, Y. Hou (2010). Development of large helium cryogenic system. *Cryogenics* 4, 18-23.
- Zhang, K., J. Li, B. Yu, D. Han and Y. Chen (2019). Fast prediction of the replacement process of oil vapor in horizontal tank and its improved safety evaluation method. *Process Safety and Environmental Protection* 122, 298-306.